Delineating faults using multi-trace seismic attributes: Example from offshore Niger Delta

Babangida Jibrin[1], Yelwa N.A[2]

[1](Department of Geology and Mining, Ibrahim Badamasi Babangida University, Lapai, Nigeria)
[2](Department of Geology, Usmanu Danfodiyo University, Sokoto, Nigeria)

Abstract: *Techniques for delineating faults have been applied to a 3D seismic data acquired over parts of offshore Niger Delta. The volumetric dip and azimuth of the seismic traces was first computed directly from the seismic reflection data. Noise cancellation techniques were then applied to the data to highlight overall structural dip trend. An attribute that highlight seismic discontinuities based on trace-trace similarity was then computed over a user-defined window using the seismic reflectivity and smoothened dip data as input. The dip and similarity volumes reveal a structural framework consisting of a major NE-SW trending lineament separating two zones of contrasting structural styles. In the northern part of the lineament, deformation is compressional, with NNE-SSW to N-S trending thrusts and folds. In the south, deformation is characterized by a network of predominantly NW-SE trending extensional faults. Although the structural trend is clearly evident in the computed dip volumes, estimating multi-trace similarity along structural dips has significantly improved the ability to recognize faults in the data.*
Keywords: *Niger Delta, 3D seismic data, dip-steering, multi-trace similarity, fault detection*

I. Introduction

Mapping faults for subsurface structural modeling is the ultimate objective of most routine seismic interpretation workflows. Faults are usually thought of and interpreted as simple through-going surfaces. However, faults are zones of deformation with complex geometry and internal architecture. Thus the main challenge in mapping faults using seismic data is the ability to clearly resolve fault and fault zone geometry that the seismic reflection data may not show. In the past several seismic attributes have previously been used to highlight structural and stratigraphic features using several techniques that highlight discontinuities [1,2,3,4,5]. Faults are important in oil and gas exploration as a conduit and or barrier to the flow of hydrocarbon fluids [6,7]. In recent years, considerable exploration efforts have focused on offshore Niger Delta. As the need to discover new hydrocarbon reserves in these areas is intensified, accurate detection and mapping of faults using advanced seismic attribute computation techniques will become even more important. Reliable interpretation of faults can provide the interpreter a very powerful tool for mapping and visualizing complex subsurface geological structures. This paper presents a workflow for improved detection of faults imaged in a 3D seismic data acquired over parts of the north-western offshore Niger Delta in water depths of up to 2000m (Fig 1). Horizontal (time slice) and vertical cross sectional views through the computed attribute volumes are used to show that the quality of fault detection has been significantly enhanced using the techniques applied to the data.

II. Methodology

2.1 Data

The 1600 km^2 post-stack time-migrated 3D data have an inline and crossline spacing of 12.5m and 18.75m respectively. The recording interval is 8.7s with a 4ms sampling rate. The data are displayed with a reverse polarity and have been zero-phased migrated with vertical scale in seconds (s) two-way travel time. Spectral analysis shows that the dominant frequency bandwidth range from 25 to 60Hz between 2.5 and 5.0s two-way travel time in the shallower sections (Fig 2a), and 8 to 20Hz between 5.0 and 8.7s two-way travel time in the deeper sections (Fig 2b). The maximum vertical resolution is ~10m (48Hz) in the former and ~60m (10Hz) in the latter. Vertical resolution was computed using extrapolated velocities from an interval velocity plot of the offshore Niger Delta [8]. The loss of seismic resolution is usually attributed to loss of high frequency events with depth in addition to fluid overpressures especially in Tertiary deltaic environments [9]. The workflow for improving the quality of the data for fault detection is summarized in Fig 3.
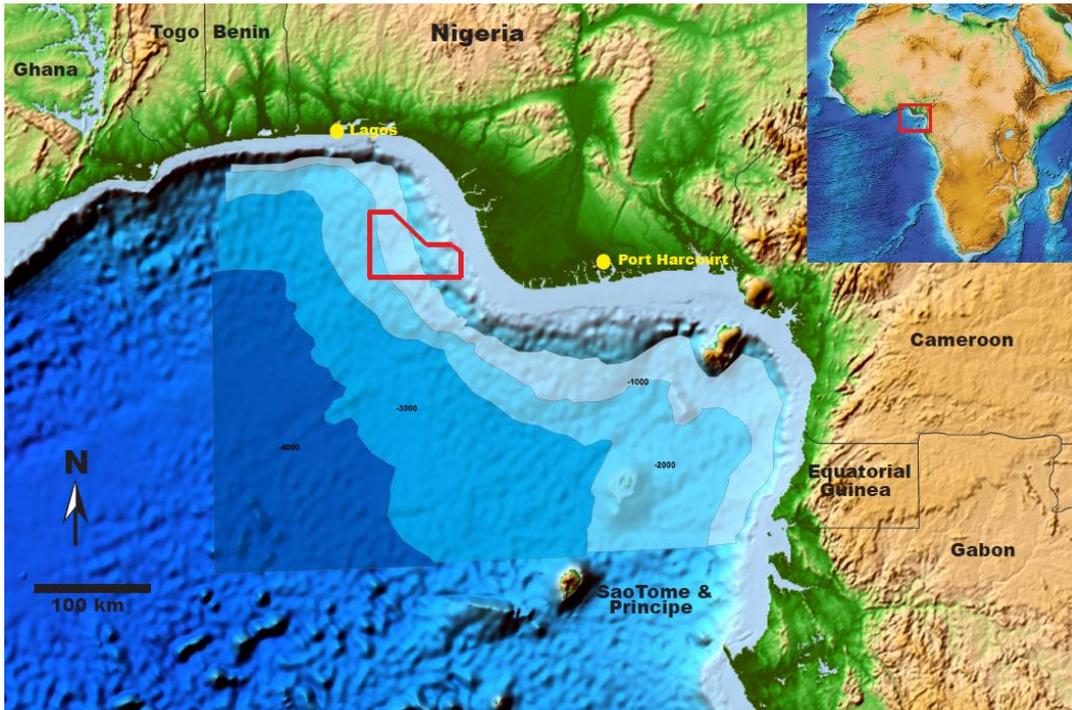

Fig 1: Shaded relief and bathymetric map of the Gulf of Guinea showing the location of the study area.
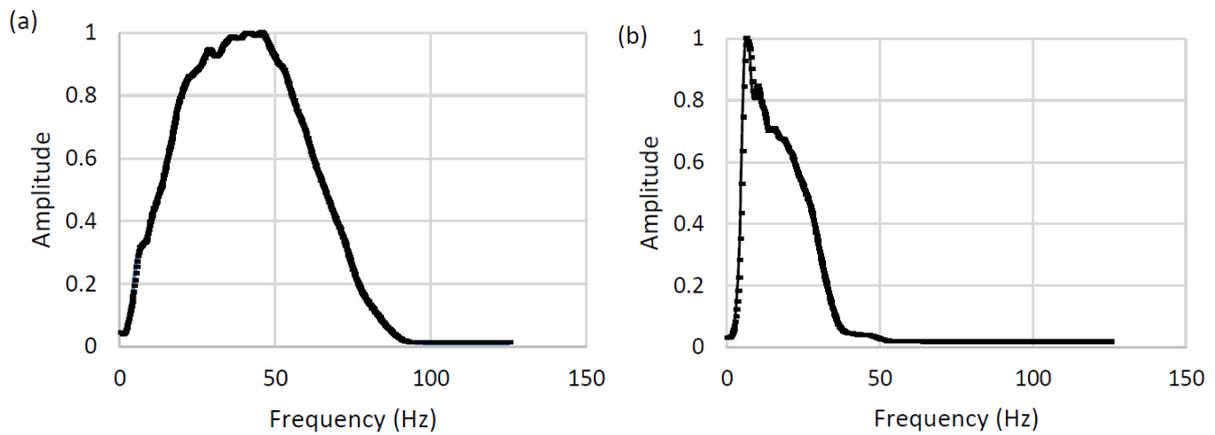

Fig 2: Frequency bandwidth extracted between 2.5 and 5.0s (a), 5.0 and 8.7s (b) two-way travel times.
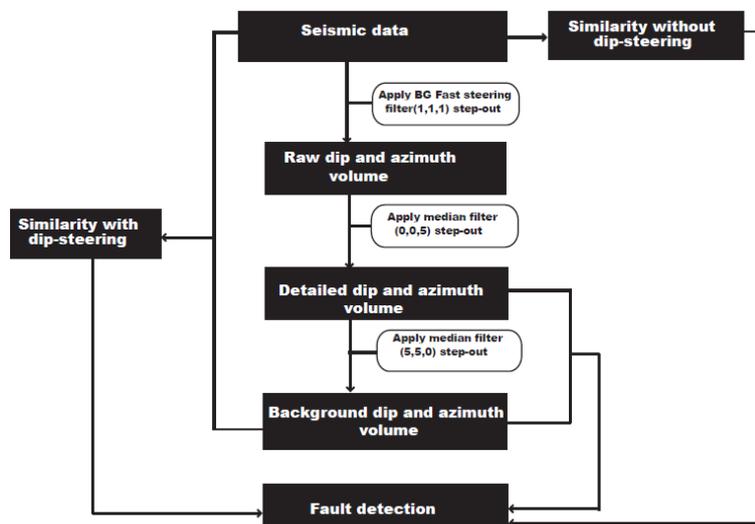

Fig 3: Workflow for delineating faults in the data.

2.2 Background theory
2.2.1 Computing multi-trace similarity

An attribute that detects and highlights the waveform similarity of neighboring trace pairs and the time difference between the traces interpreted as vectors was computed to highlight structural features. Similarity is mathematically the Euclidean distance in hyperspace between vectors of the segments, normalized between 0 and 1 to the sum of the lengths of the vectors. A high similarity means the trace segments are similar in wave-shape and amplitude i.e. similarity values are identical and no structural features are apparent. Low similarity implies that the neighboring traces are dissimilar probably due to distortions caused by structural deformation [10].

2.2.2 Dip-steering volume computation

Similarity is sensitive to amplitude differences between trace segments in addition to wave-shape. The difference in the response of the attribute at the location of faults is largely dependent on the dip of the traces. By applying dip-steering techniques, similarity computation is along trace-to-trace guided by the local dip and azimuth at every position along the track (Fig 4a). However, the trace segments are aligned horizontally without the application of dip-steering (Fig 4b). For improved detection of faults and fault zones, the application of dip-steering reduces the sensitivity of similarity to dipping reflectors with no apparent link to faulting by aligning adjacent trace segments with a lag time.
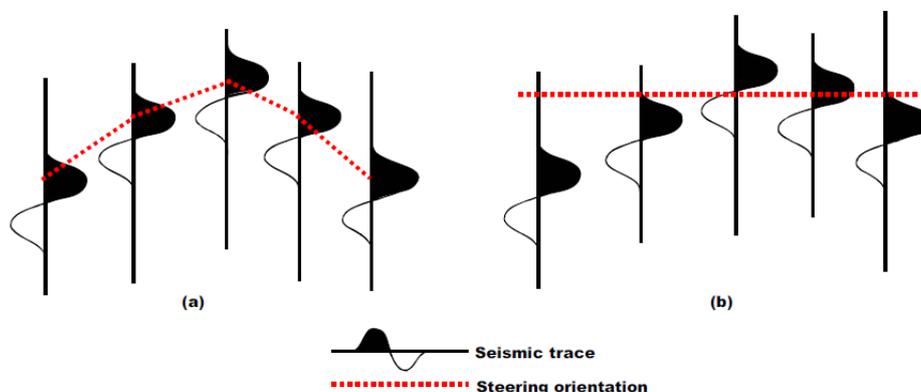

Fig 4: Cross sectional schematic illustration of dip-steering computation applied to the data (Tingdahl, 2003).

The first dip-steering volume was calculated directly from the seismic data using a fast steering filter algorithm based on the analysis of the vertical and horizontal gradient of the amplitude data. Three samples, one each in the inline, crossline and time directions were used for the computation (I.e. step-out is 1,1,1). The filtering distance is 37.5m in the inline direction (Inline spacing of 12.5 x number of samples) and 56.25m in the crossline direction (Crossline spacing of 18.75m x number of samples). In the time (Z) direction the filtering length is 12ms (Sampling rate of 4ms x number of samples). This data is referred to as the "raw dip and azimuth volume" (Fig 5b).

The second dip-steering data was computed by applying edge preserving median filter to the raw dip-steering volume in the temporal (Vertical direction) to attenuate localized noise along structural dips. The filtering distance is 20ms in the temporal direction. This data contain localized multi-trace dip and azimuth and is the "detailed dip and azimuth volume" (Fig 5c). The third steering data was computed by applying edge preserving smoothing filter to the detailed dip-steering volume in the inline and crossline directions to smoothen localized noise using ten samples along a filtering distance of 125m in the inline direction (Inline spacing is 12.5 x number of samples) and 187.5m in the crossline direction (Crossline spacing is 18.75 x number of samples). No filtering was applied in the temporal direction. This data is the "background dip and azimuth volume" (Fig 4d). The data are displayed in grey-scale (Fig 4b, Figs 6c-d) with low dips represented by white (Positive dips) and high dips are represented by black (Negative dips).The parameter setting applied to computing the dip-steering data are summarized in Table 1. Comprehensive description of the algorithm applied to the data can be found in Tingdahl [10,11].

Table 1: Parameter setting for computing dip and azimuth of the seismic traces

Input data	Filter step-out	No. of samples	Filter type	Output data
Seismic reflection	(1,1,1)	Three (One each in the inline, crossline and time directions)	Median	Raw steering
Raw dip and azimuth	(0,0,5)	Five (all in the time direction only)	Median	Detailed steering
Detailed dip and azimuth	(5,5,0)	Ten (Five in the inline and five in the cross line directions only)	Median	Background steering

2.2.3 Computing multi-trace similarity

The input data for computing multi-trace similarity are the seismic reflection and background dip and azimuth volumes. For this study, a time gate of + 24ms and -24ms, equivalent to the average seismic wavelength within the window of investigation and a step-out of 1,1 (I.e. two samples), one sample each in the inline and crossline directions were used in computing multi-trace similarity. This implies that similarity was computed along every inline and crossline steered by background dip and azimuth. Multi-trace similarity was not computed in the temporal (Vertical direction) in order to minimize artifacts along time slices that can potentially mask structural features of interest (Marfurt, personal communication). All trace pairs defined by the Inline, crossline and time position were computed using the full-block extension. Minimum similarity was selected as the output statistical operator so that dissimilarity values close to 0 are highlighted. The data are displayed in grey-scale with the darker shades indicating areas of dissimilar seismic traces, while the lighter shades indicate similar seismic traces (Fig 6). The parameter setting for multi-trace similarity computation is presented in Table 2. Comprehensive description of the mathematics of multi-trace similarity computation as applied to the data is discussed in [10,11,12].

Table 2: Parameter setting for computing multi-trace similarity

Input data	Time gate (ms)	Extension	Trace step-out	No. of samples	Dip-steering	Statistical output operator	Output data
Seismic reflection	(-24,24)	Full block	(1,1)	One each in the inline and crossline directions only	None	Minimum	Similarity without dip-steering
Seismic reflection and background dip and azimuth	(-24,24)	Full block	(1,1)	One each in the inline and crossline directions only	Full steering	Minimum	Similarity with dip-steering

3   Results and discussion

The workflow described above has been applied to the data and the results are shown in Figs 5 to 8. Fig 4a shows the input seismic data and Figs 5b-c is the output dip-steering volumes. The red and yellow arrows in fig 5 highlight major dip anomalies hardly seen in Fig 5a. The green arrows highlight NNE-SSW trending positive dip and low reflectivity anomalies. These anomalies terminate against a linear zone of NE-SW trending positive dip and low reflectivity anomaly (Black arrow). Similar anomalies trending NW-SE are also seen in the south-eastern parts of the area (Red arrows and circle). In general, filtered dip volumes highlight subtle pattern of deformation in the context of the overall structural trend. Fig 6 are time slices extracted at 3.7s two-way travel time to show the usefulness of computing multi-trace similarity along structural dips (Using dip-steering). In Fig 6a, similarity was computed directly from the seismic data without applying dip-steering, while in Fig 6b multi-trace similarity was computed with dip-steering (Using sub-regional dip data). The contrast of the major and minor discontinuities is clearly higher in the latter.

In vertical cross sectional view, faults are recognized by break in the continuity of seismic reflection corresponding with discrete zones of low similarity (Red arrows in Fig 7 and Fig 8). The faults in Fig 7 have a reverse sense of displacement (Red arrows), while in Fig 8 fault displacement is predominantly normal (Green arrows). The green arrow in Fig 7 indicates the vertical cross sectional view of the major NE-SW trending lineament zone (Black arrows in Fig 6). Comparing similarity computed using dip-steering with similarity computed directly from the seismic, the contrast of the shallow and deeper faults in vertical cross sectional view is significantly higher in the former (Fig 7c and Fig 8c). Furthermore, the visibility of the complex zone of faulting has been improved with the application of dip-steering (Green arrows in Fig 7 and Fig 8). Computing multi-trace similarity using dip-steering techniques has also corrected the anomalously low similarity due to dipping reflectors. This has resolved the real structure of the dipping reflectors (Yellow circles in Fig 7c and Fig

8c). Without the application of dip-steering, the anomalously low similarity in the forelimb and back limbs of the fault would have been interpreted as due to structural deformation.

The seismic attribute data highlight two distinct pattern of deformation partitioned by a NW-SW trending lineament zone. In the northern part of the lineament, deformation is compressional with series of regularly-spaced seaward-verging NNE-SSW trending thrust faults and folds. These thrusts are in places cross cut by trending E-W and NW-SE normal faults (Fig 5b). In the southern parts of the lineament, deformation is predominantly extensional with a dense network of NW-SE trending array of up faulted and down faulted blocks (Red arrows in Fig 8c) similar to graben and horst. Although evidences of folding and thrusting can be seen in the data (Yellow circles in Fig 8c), the structural configuration is clearly not evident in the input seismic amplitude data.
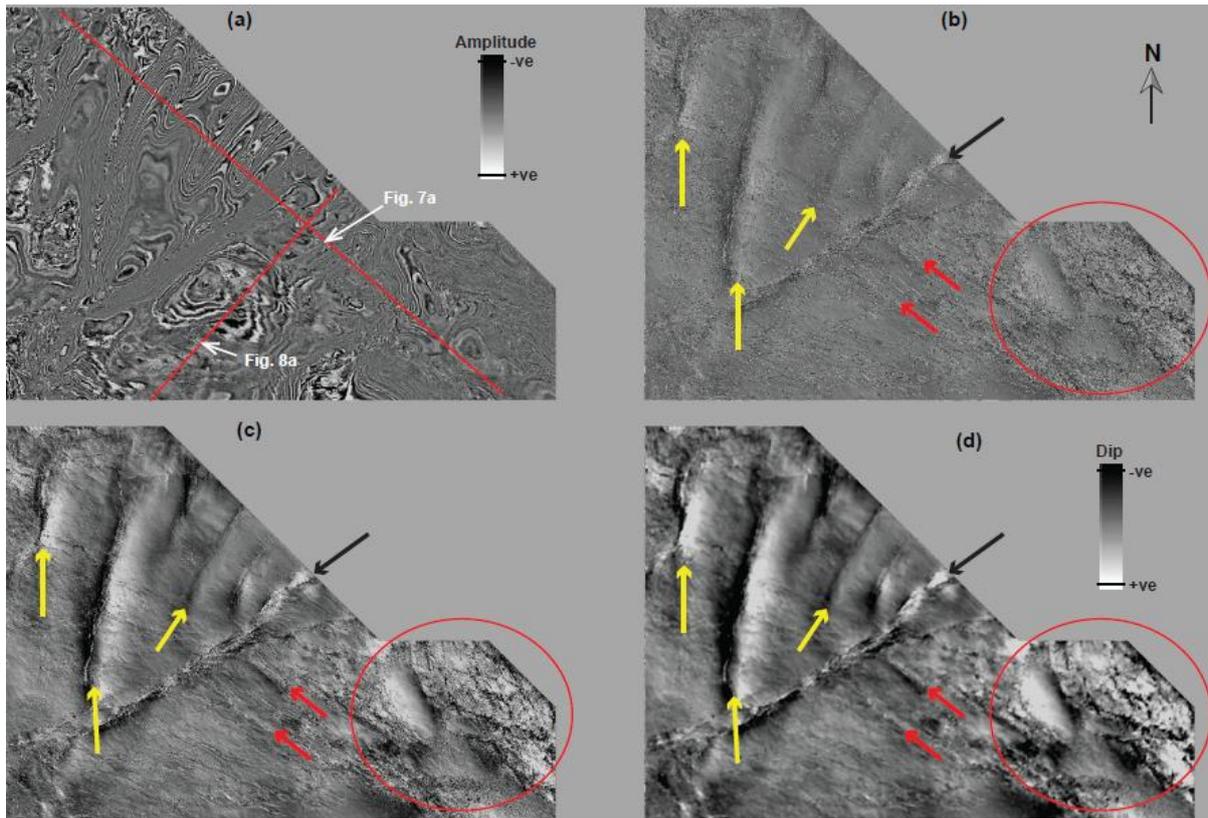

Fig 5: Time slices at 3.7s two-way travel time through seismic volume (a) raw dip and azimuth volume (b), detailed dip and azimuth volume (c), and background dip and azimuth volume (d). The cross sections in part (a) are shown in Fig 7a and Fig 8a.
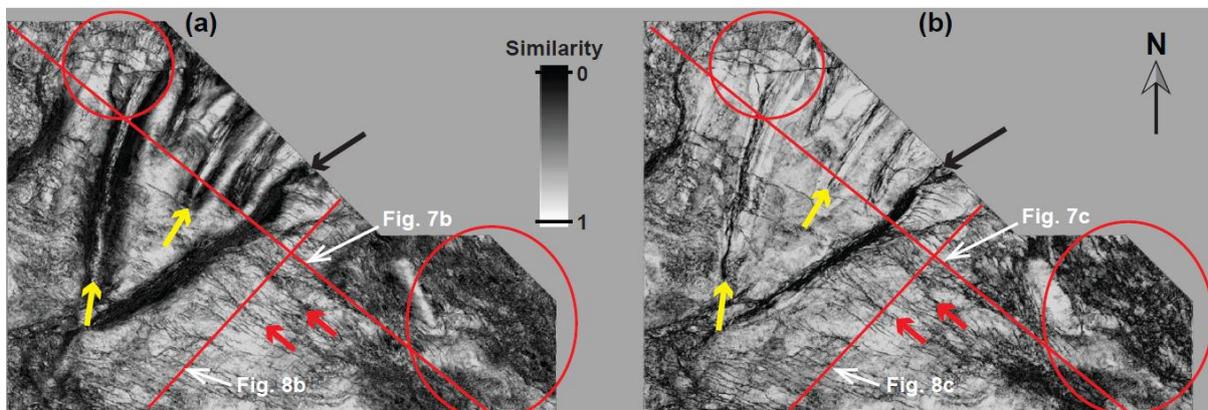

Fig 6: Time slice extracted at 3.7s two-way travel time through multi-trace similarity attribute computed directly from seismic data without dip-steering (a) and with dip-steering (b). The cross sections in part (a) and part (b) are shown in Fig 7 and Fig 8 respectively.
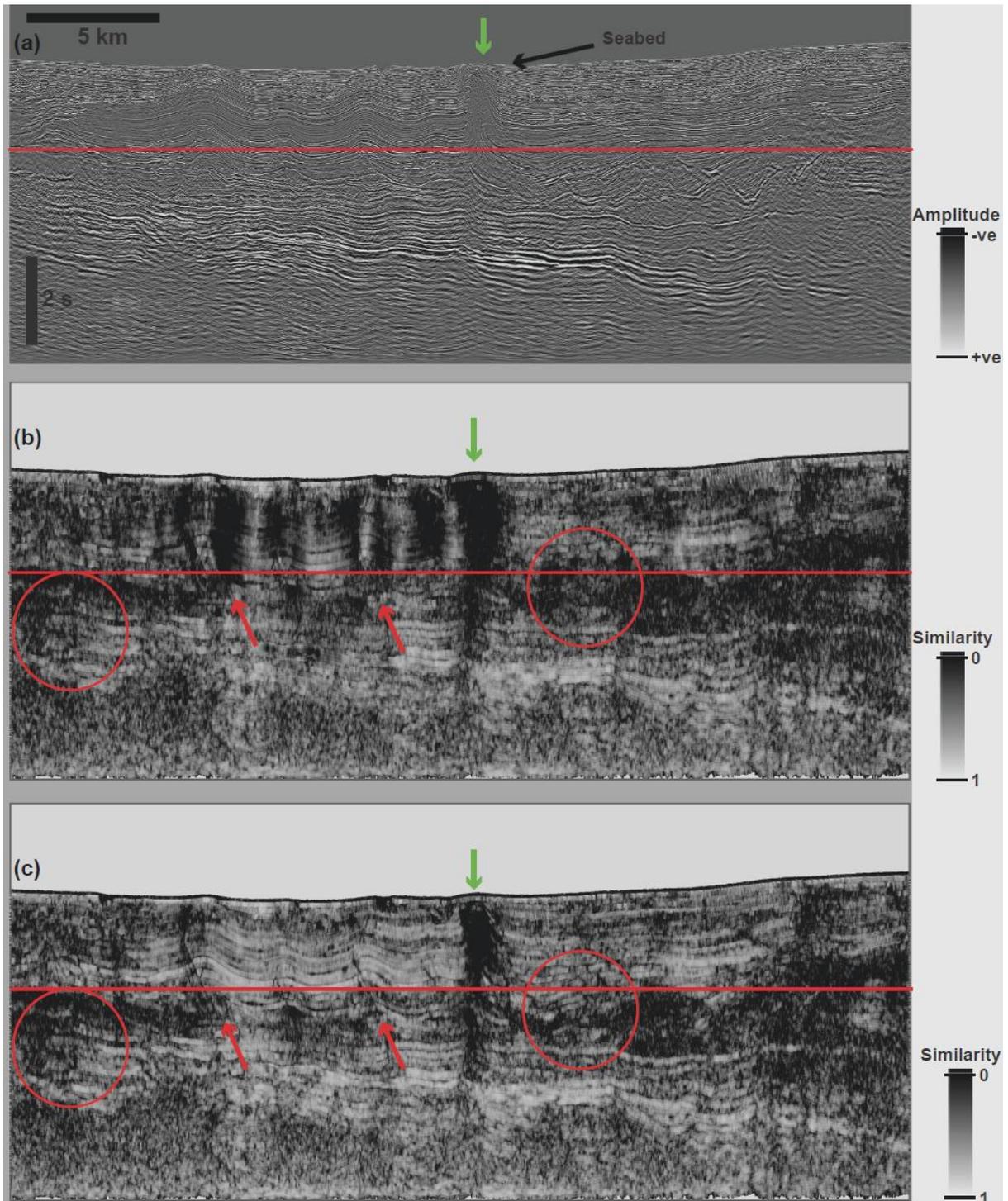
Fig 7: Vertical cross sectional views of seismic reflection (a), multi-trace similarity attribute computed without dip-steering (b), and with dip-steering (c). The red line is the location of time slices at 3.7s two-way travel time through the data volumes. Vertical scale is in seconds (two-way travel time) and horizontal scale is in kilometers. Vertical exaggeration is ~x2 the horizontal scale.
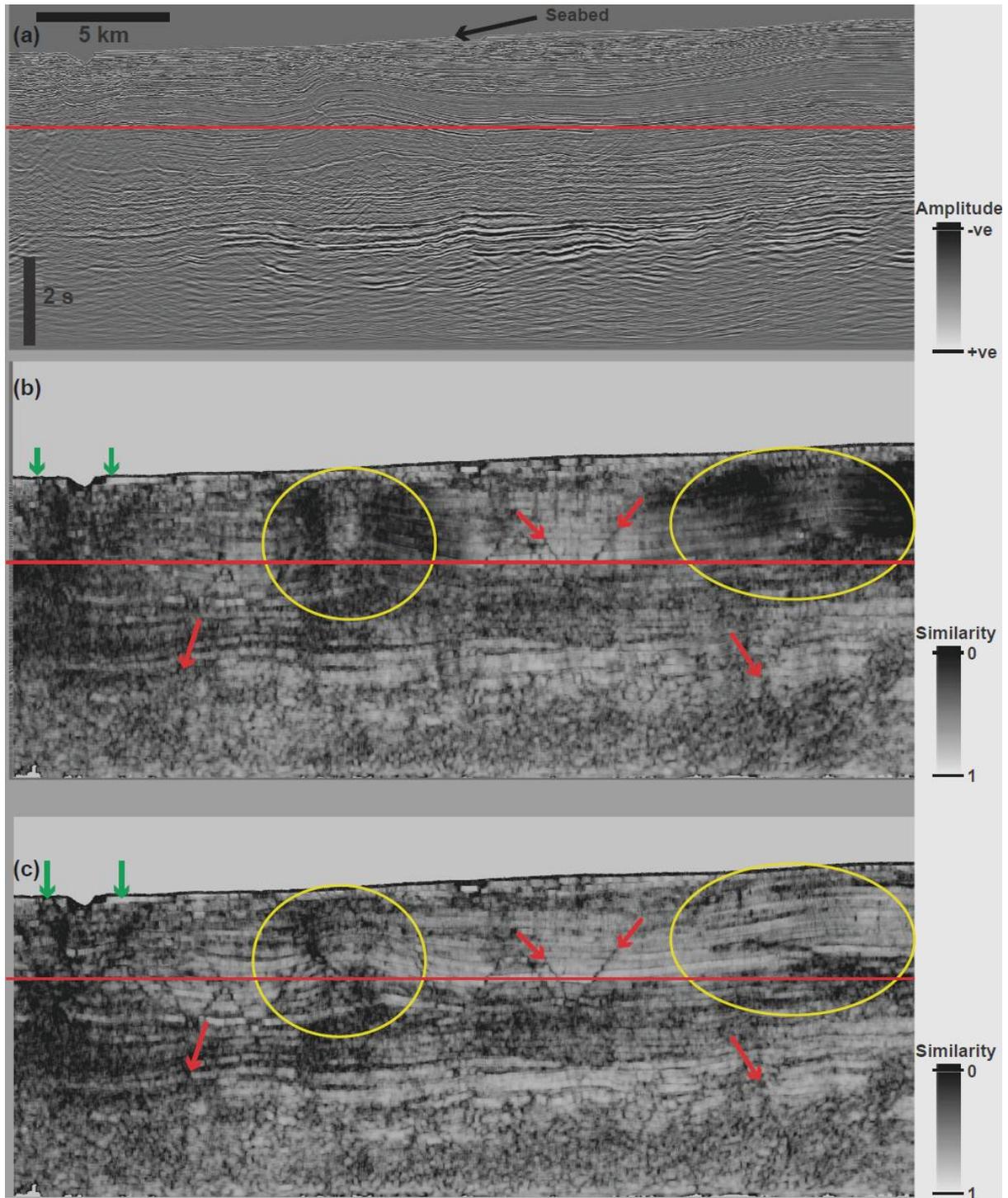
Fig 8: Vertical cross sectional views of seismic reflection (a), multi-trace similarity attribute computed without dip-steering (b), and with dip-steering (c). The red line is the location of time slices at 3.7s two-way travel time through the data volumes. Vertical scale is in seconds (two-way travel time) and horizontal scale is in kilometers. Vertical exaggeration is ~x2 the horizontal scale.

4   Conclusion

Seismic attribute computation techniques using offshore Niger Delta 3D seismic data reveal a major zone of strike-slip faulting trending NE-SW that separates two distinct structural domains. Cross sectional views through the data volumes show that faults and fault zone contrast have been significantly enhanced by computing multi-trace similarity using dip-steering.

Acknowledgements

References

[1]. Bahorich, M.S., and S.L., Farmer, 3-D seismic coherency for faults and stratigraphic features, The Leading Edge, 14, 1995, 1053-1058.

[2]. Marfurt, K.J., V. Sudakher, A. Gerszenkorn, K.D. Crawford, and S.E. Nissen, Coherency calculations in the presence of structural dips, Geophysics, 64, 1999, 104-111.

[3]. Al-Dossary, S., and K.J. Marfurt, 3D volumetric multi-spectral estimates of reflector curvature and rotation, Geophysics, 17, 2006, 41-45.

[4]. Chopra, S., and K.J., Marfurt, Coherence and curvature attributes on pre-conditioned seismic data, The Leading Edge, 30, 2011, 386-393.

[5]. Qayyum, F., and P. de Groot, Seismic dips help unlock reservoirs, American Oil and Gas Reporter, 2012, 75-79.

[6]. Knipe, R.J., G. Jones, and Q.J. Fisher, Faulting, fault seal and fluid flow in hydrocarbon reservoirs: an introduction, Geological society of London Special Publication, 1998, 147, VII-XXI.

[7]. Sorkhabi, R., and Y. Tsuji, The place of faults in petroleum traps, in Sorkhabi, R. and Y. Tsuji, (Ed), Faults, fluid flow and petroleum traps (American Association of Petroleum Geologists Memoir, 2005) 85, 1-31.

[8]. Cobbold, P.R., C.J. Benjamin, and L. Helge, Structural consequences of fluid overpressure and seepage forces in the outer thrust belt of the Niger Delta, Petroleum Geoscience, 15, 2009, 3-15.

[9]. Maloney, P.D., Seismic analysis of the Niger Delta gravitational detachment systems, doctoral diss., Durham University, 2011.

[10]. Tingdahl, K.M., Improving seismic chimney detection using directional attributes, Developments in Petroleum Science, 51, 2003, 157-173.

[11]. Tingdahl, K.M., and P. de Groot, Post-stack dip and azimuth processing, Journal of Seismic Exploration, 12, 2003, 113-116.

[12]. Tingdahl, K.M and M. de Rooij, Semi-automatic detection of faults in 3-D seismic data, Geophysical prospecting, 53, 2005, 533-542.